

# Several micron range measurements with sub-nanometric resolution by the use of dual-wavelength digital holography and vertical scanning

Tristan Colomb<sup>a</sup>, Jonas Kühn<sup>b</sup>, Christian Depeursinge<sup>b</sup> and Yves Emery<sup>a</sup>

<sup>a</sup> Lyncée Tec SA, PSE-A, CH-1015 Lausanne

<sup>b</sup>Ecole polytechnique fédérale de Lausanne, Institute of imaging and applied optics, CH-1015 Lausanne, Switzerland

## ABSTRACT

Reflection digital holographic microscopy (DHM) is a very powerful technique allowing measuring topography with a sub-nanometer axial resolution from a single hologram acquisition. But as most of interferometer methods, the vertical range is limited to half the wavelength if numerical unwrapping procedure could not be applied (very high aspect ratio specimen). Nevertheless, it was already demonstrated that the use of dual-wavelength DHM allows increasing the vertical range up to several microns by saving the single wavelength resolution if conditions about phase noise are fulfilled (the higher the synthetic wavelength, the smaller the phase noise has to be). In this paper, we will demonstrate that the choice of a synthetic wavelength of about 17 microns allows measuring precisely a  $4.463\mu\text{m}$  certified step. Furthermore, we will show the feasibility of a sub-nanometer resolution on a range higher than the synthetic wavelength by being able to map the dual-wavelength measurement on data acquired from a vertical scanning process, which precision is about  $1\mu\text{m}$ .

**Keywords:** Digital holography, microscopy, dual-wavelength

## 1. INTRODUCTION

As one knows, digital holographic microscopes (DHM) allow retrieving quantitative information of object wavefront by the numerical reconstruction of its amplitude and phase from a digital hologram recorded by a CCD or CMOS camera.<sup>1-3</sup> Thanks to its interferometric nature, DHM has an axial resolution less than  $\lambda/150$ . However, the very sensitive information provided by the phase has by essence the downside to be only defined modulo  $2\pi$ , as expressed in

$$\varphi(x, y) = 2\pi \left\{ \frac{OPL(x, y)}{\lambda} - E \left[ \frac{OPL(x, y)}{\lambda} \right] \right\} \quad (1)$$

with  $E(x)$  being the integer part of  $x$ .

As a consequence of Eq.1, the periodic nature of the phase information results in a so-called phase ambiguity when objects with optical path lengths (OPL) larger than the laser wavelength (400-700 nm for the visible range) are considered. For a vast majority of situations, so-called unwrapping algorithms can be used to retrieve the true topography, but they may fail for high aspect-ratio structure (e.g. a step) or high-roughness surfaces, as well as noisy experimental conditions or absence of signal in some regions of the field-of-view (FOV). In such cases, DHM applications range (or so-called dynamic range) can be described as limited to small OPL samples, about half the wavelength in topology. A small handout of typical examples of situations where standard unwrapping algorithms are to be used, with both successful and unsuccessful results is presented in Fig.1. More evolved unwrapping algorithms could sometimes diminish or suppress artefact on edge regions seen for example on Fig.1f,h; but these algorithms could not suppress  $2\pi$  ambiguity if the elements are higher than half the wavelength. A solution to overcome this reduced range of measurement is to use a second wavelength, the dual-wavelength DHM permits to synthesize the measurement with a several microns wavelength.

---

Further author information: (Send correspondence to Tristan Colomb)  
E-mail: tristan.colomb@lynceetec.com, Telephone: +41 21 693 02 27

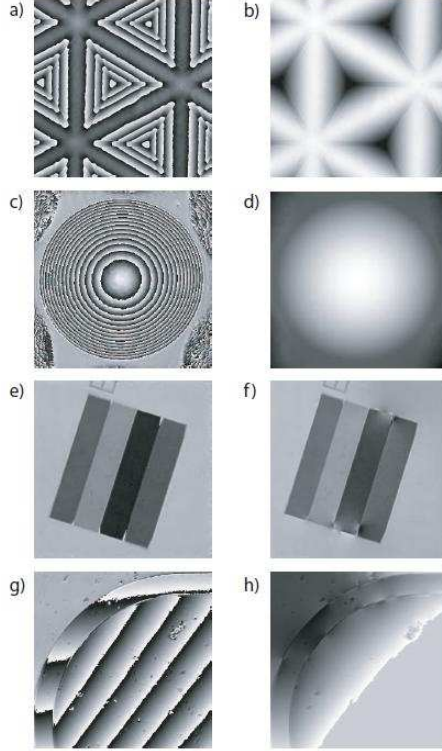


Figure 1. Behavior and limitations of unwrapping algorithms. (a-d) Successful 2-D unwrapping on phase images of a micro-corner cubes array, respectively an aspherical microlens; (e) Phase image of a up to  $1.2\mu\text{m}$  high Silicium gold-coated staircase sample obtained in reflection with clear phase ambiguities; (f) Erroneous 2-D unwrapping of (e) with phase ambiguities still remaining and failures in some edge regions; (g) Phase image of a moving MEMS micro-mirror with phase jumps in presence of dust particles and structure edges; (h) Failing 2-D unwrapping of (g) with white saturation region removed for better visibility.

## 2. DUAL-WAVELENGTH APPROACH

### 2.1 Dual-wavelength interferometry

Already back in 1947, Forrester et al. published the first concept of beat wavelength applied to light frequencies,<sup>4</sup> in the presence of two nearby frequencies waves. The principle relies on the superposition of two mutually-incoherent interference regimes at two different frequencies, resulting in the appearance of a so-called Moiré pattern. A schematic of the phenomena for a 1-D interference superposition is represented in Fig. 2 for two sinusoidal waves at different frequencies.

Now the idea behind beat-wavelength interferometry is to retrieve the phase of the envelope signal depicted in bold in Fig. 2(b), also called beat signal. Indeed, this beating signal is obviously much slowly varying due to its higher period, thus the phase ambiguity-free range should be much more extended. Mathematically the beat signal phase  $\phi$  is obtained by computing the phase difference between both original phases, as expressed in Eq. 2 in our holographic context.

$$\Phi = \varphi_1 - \varphi_2 = \frac{2\pi OPL(z)}{\lambda_1} - \frac{2\pi OPL(z)}{\lambda_2} = \frac{2\pi OPL(z)}{\Lambda} \quad (2)$$

with  $OPL(z) = 2z$  for reflection measurements of the topography  $z$ , and  $\Lambda$  is the so-called "beat-wavelength" defined by:

$$\Lambda = \frac{\lambda_1 \lambda_2}{|\lambda_2 - \lambda_1|} \quad (3)$$

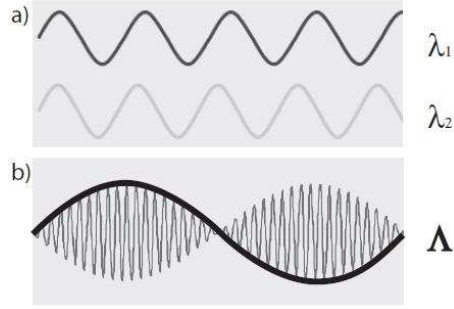


Figure 2. Moiré pattern phenomena when mixing two different close-wavelength signals. (a) Schematic of two sinusoids with close frequencies; (b) Resulting pattern when superposing the two signals of (a), with high frequency oscillations modulated by a slowly-varying envelop.

Clearly from Eq. 3, the smaller the wavelength gap  $\lambda_2 - \lambda_1$ , the higher the beat wavelength  $\Lambda$  and the range in which its phase  $\phi$  does not suffer from phase ambiguity. The phase  $\phi$  is often called synthetic phase because it does not correspond to any real signal, as there is no interference between the two wavelength signals. This is important because, despite some usual oral shortcut describing the signal behavior as if a source of wavelength  $\Lambda$  were used, a huge hypothesis is made in Eq. 2: the wavelength dependency of the OPL is neglected. A dependency could occur for example for non-homogenous sample reflection measurement. Indeed the substrate complex refractive index  $n$ , could introduce a possible wavelength dependency. Regarding the state-of-the-art, dual-wavelength methods were first applied in classical holography by Hildebrand<sup>5</sup> and Zelenka<sup>6</sup> for contouring by simultaneous illumination, and later by Wyant for the two-wavelength holographic (TWH) testing of aspherics by single or double exposure.<sup>7</sup> Then Polhemus<sup>8</sup> generalized the concept of two-wavelength interferometry in static or dynamic configurations. Naturally, a large field of application of two-wavelength interferometry can be found in absolute distance measurement<sup>9,10</sup> by heterodyne or super-heterodyne detection, large step height measurement<sup>11,12</sup> or rough surface investigation by speckle detection.<sup>13</sup> In top of the heterodyne detections methods, information retrieval from Moiré patterns can also be achieved by Fourier transform methods,<sup>14</sup> time-sharing sinusoidal modulation of laser diodes.<sup>15</sup>

## 2.2 Dual-wavelength in digital holography

Dual-wavelength digital holography was first introduced by Pedrini *et al.*<sup>16</sup> and Wagner *et al.*<sup>17</sup> by subtraction of two reconstructed phase maps obtained with either pulsed ruby or scanning dye laser to perform a millimeter contouring of the object. Recently, Kims group proposed a similar technique within the framework of DHM in order to remove the phase ambiguity of digitally-propagated wavefronts.<sup>18,19</sup> Such different wavelengths phase maps subtraction in the sense of Eq. 2 requires achromatic setups, otherwise numerical image resizing is needed, as explained in Refs. 20,21. Instead of using two different laser sources, it is also possible to use the mode-hop of a laser diode to change the wavelength,<sup>22</sup> or even to generate a millimeter-range wavelength with a terahertz source<sup>23</sup> (but this is not a dual-wavelength method).

Most of published two-wavelengths digital holography techniques require a sequential approach to record the information from both sources, with repeated acquisitions for each wavelength. This prevents real-time dual-wavelength measurements because at least two camera acquisitions are needed. Kühn *et al.* proposed a real dual-wavelength by recording a hologram with two different propagations for two different wavelength reference waves.<sup>24</sup> When analyzing the hologram in its frequency domain, two different spatial carrier frequency can be filtered to reconstruct separately the two different numerical waves. In this paper, we register two different holograms successively at different wavelength, but there is no restriction for the method to be used with simultaneous record.

## 2.3 Recording principle

Let us take the example of two holograms successively acquired by a digital camera, with two collinear object beams  $\mathbf{O}_i$  and at two different wavelengths  $\lambda_i$  ( $i = 1, 2$ ) and that interfere with the reference beam  $\mathbf{R}_i$ , in an off-axis configuration like depicted in Fig. 3.

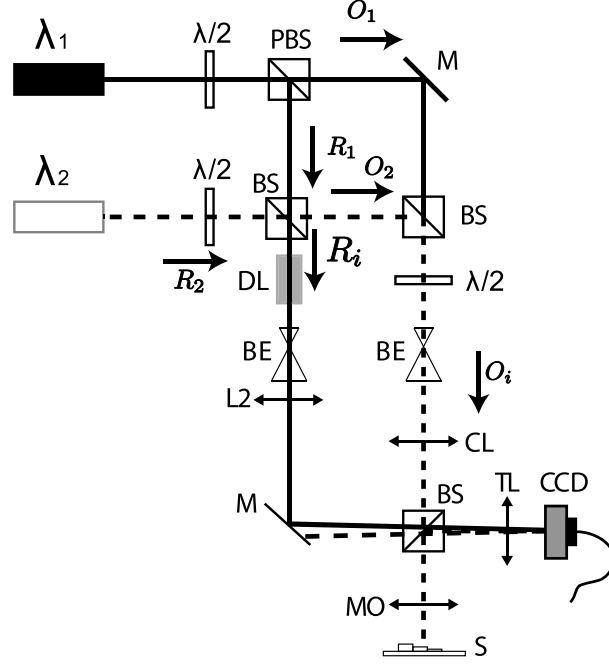


Figure 3. Dual-wavelength DHM experimental setup.  $\lambda/2$ : half-waveplate; M: mirrors; PBS: polarizing beamsplitter; BS: non-polarizing beamsplitter; DL: delay line, BE: beam-expander with pinhole-based spatial filtering; L: lens; CL: condenser lens; MO: achromatic microscope objective; S: specimen; TL: tube lens.

The two intensity patterns on the CCD can be expressed as

$$I_{H,i}(x, y) = |\mathbf{R}_i|^2 + |\mathbf{O}_i|^2 + \mathbf{R}_i \mathbf{O}_i^* + \mathbf{R}_i^* \mathbf{O}_i, \quad (4)$$

with  $I_{H,i}$  being the hologram intensities for  $\lambda_i$  ( $i = 1, 2$ );  $x, y$  the coordinates in the camera plane, and  $*$  denoting the complex conjugate. The first two terms in Eq. 4 correspond to the zero order of diffraction. The last two terms correspond to the interference of the object wavefronts  $\mathbf{O}_i$  (the virtual images), or their conjugate  $\mathbf{O}_i^*$  (the real images), with the reference waves. With  $\mathbf{O}_i$  collinear on the optical axis, the carrier frequencies are dependent on the k-vectors of  $\mathbf{R}_i$  and could be easily filtered in the Fourier domain:<sup>25</sup>

$$I_{H,i}^F = \mathbf{R}_i^* \mathbf{O}_i. \quad (5)$$

## 2.4 Dual-wavelength reconstruction

### 2.4.1 Individual wavefront propagation

Once both wavelength wavefronts in the hologram plane are retrieved by spatial filtering, it is possible to numerically propagate them successively.

Taking these two filtered holograms as  $I_{H,1}^F$  for  $\mathbf{R}_1^* \mathbf{O}_1$  and  $I_{H,2}^F$  for  $\mathbf{R}_2^* \mathbf{O}_2$ , then using the convolution formulation,<sup>20</sup> we obtain the expression of Eq. 6 for the dual-wavelength propagation:

$$\Psi_i(m, n) = A \cdot \Gamma_{I,i} \cdot \text{FFT}^{-1} \left\{ \text{FFT} [\Gamma_{H,i} I_{H,i}^F] e^{-i\pi\lambda_i d_i (\nu_k^2 + \nu_l^2)} \right\} \quad (6)$$

where  $\Psi_i$  is the reconstructed wavefront for wavelength  $\lambda_i$  in the convolution formulation,  $d_i$  is the propagation distance for wavelength  $\lambda_i$  and  $\Gamma_{j,i}$  ( $j$ =Hologram, Image plane) the numerical lens used for aberration compensation.

The formulation of Eq. 6 enables to propagate each wavefront  $\Psi_i$  in an independent manner: phase aberrations (tilt, defocus...) or chromatic aberrations could be compensated differently by the adjustment of numerical lenses (NLs) and reconstruction distances  $d_i$ .<sup>20,26</sup>

### 2.4.2 Beat-wavelength phase reconstruction

At this point, the two reconstructed complex wavefronts  $\mathbf{O}_1$  and  $\mathbf{O}_2$  in the image plane contain information both in amplitude and in phase, providing a nanometer-scale resolution in the vertical axis but suffering from phase ambiguity for OPLs larger than the wavelength. Based on Eq. 2, the calculation of  $\mathbf{O}_1 \mathbf{O}_2^*$  in the reconstruction plane allows to obtain the expression of Eq. 7 for the synthetic wavelength phase  $\Phi$ .

$$\Phi = \arg(\mathbf{O}_1 \mathbf{O}_2^*) = \varphi_1 - \varphi_2 = 2\pi \frac{x}{\lambda_1} - 2\pi \frac{x}{\lambda_2} = 2\pi x \left( \frac{\lambda_2 - \lambda_1}{\lambda_1 \lambda_2} \right) = \pm 2\pi \frac{x}{\Lambda}, \quad (7)$$

where  $x = OPL(z)$ , for example in reflection  $x = 2z$ ,  $\varphi_i$  is the reconstructed phase for the wavelength  $\lambda_i$ , and  $\Lambda$  is the synthetic beat wavelength defined as in Eq. 3.

As already explained above, the beat wavelength  $\Lambda$  is much larger than the original couple of wavelengths, the smaller the difference  $(\lambda_2 - \lambda_1)$ , the larger the synthetic wavelength, typically within the range of micrometers to millimeters. The corresponding synthetic phase obtained with Eq. 7 therefore enables e.g. to resolve much higher structures in reflection, by removing the phase ambiguity in the range of the beat wavelength  $\Lambda$ , thus greatly increasing the range for the phase measurement.

Despite this advantage, it should be noticed that the laser sources wavelengths stability is a top-priority issue for direct synthetic wavelength imaging.<sup>27</sup> Indeed, any variation in wavelength is amplified when the raw beat wavelength phase map is computed according to Eqs. 3 and 7, and the noise on the phase  $\varphi_1$  or  $\varphi_2$  is also amplified when converted in topography due to the important value of  $\Lambda$ . Nevertheless, methods to keep the single-wavelength precision by using the synthetic phase only for phase ambiguity removal, like the ones published in Refs. 18 and 19, can potentially nullify this effect and render the technique more forgiving regarding wavelength stability.

## 2.5 Dual-wavelength reflection setup and reconstruction parameters

The measurement are achieved with a DHM R1100<sup>TM</sup> that has a Mach-Zehnder configuration reflection setup, as depicted in Fig. 3. The laser source beams pass through wavelength filters (bandwidth about 1-1.3nm), that guaranties emission at  $\lambda_1 = 682.7$  nm and  $\lambda_2 = 656.11$  nm, yielding  $\Lambda = 16.84$   $\mu\text{m}$  for the synthetic beat wavelength.

Two successive measurements are achieved by successively switch on and off the two laser sources. After reflection on the sample, the successive wavelength collinear object wavefronts are collected by the MO (infinity-corrected), and the object images are formed by the tube lens about 5 cm behind the CCD plane. A magnification x20 MO, is used in the present case. The CCD camera is a standard 8 bits black and white CCD camera with  $p_x = 6.45$   $\mu\text{m}$  pixel size. The reference arm comprise a delay line (DL) adjusted to match the optical path length of its respective object counterparts, in order to create an interference on the CCD. By tilting the mirror M, one can finely tune each k-vector incident upon the CCD camera.

Once each wavelength interference term, here the two virtual images components, is spatially-filtered from the two acquired holograms, one can use Eq. 6 to reconstruct and propagate each wavefront in the convolution formalism. By correcting for aberrations in the hologram plane before the propagation, especially the tilt, the reconstructed images are naturally centered.<sup>20</sup> This perfect superposition and the achromatic design of the object arm of the setup, allow for an accurate subtraction of the phase images (Figs. 4a-b) in the image plane to compute the phase difference image (Figs. 4c). The reconstruction distances in the experimental configuration of Fig. 3 are  $d_1 = -44.4$  mm and  $d_2 = -43.7$  mm, corresponding to the distances between the image planes and the CCD plane. As the reconstruction distances difference is very small due to the achromatic conditions, the magnification difference can be considered negligible and the superposition conditions are fulfilled.

## 2.6 Noise amplification

The experimental noise can be evaluated by measuring the phase spatial standard deviation over the field of view. For this setup, a high quality mirror has permitted to evaluate an experimental noise of about  $2^\circ$  of phase spatial standard deviation over the whole field-of-view for each phase map  $\varphi_1$  and  $\varphi_2$ . When considering the synthetic beat phase  $\Phi$ , the spatial standard deviation  $\sigma_\Phi$  raises to about  $3^\circ$ . Indeed, the latter standard

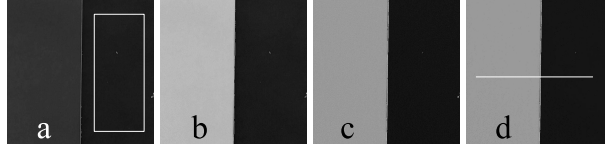


Figure 4. Phase reconstructions for (a)  $\lambda_1$  and (b)  $\lambda_2$ ; (c) phase difference. The phase offset is adjusted to have a mean value inside the white rectangle equal to -150 degrees. (d) Synthetic phase map obtained with unwrapping procedure.

deviation value for the synthetic phase is directly related to the property that the variance of the sum (or in our case a difference) of two Gaussian-noise distributions is the sum of the individual variances: we have precisely here a  $\sqrt{2}$  amplification for the standard deviation when considering the phase difference of two signals with quasi-identical standard deviations.

Concerning the axial topographic resolution in reflection, this corresponds to about  $\sigma_{zi} = 2$  nm for monochromatic standard deviation, and  $\sigma_{zs} = 70$  nm for the synthetic wavelength topographic standard deviation, which is a consequence of the noise amplification phenomena. This drawback of the method can be best understood by considering  $\sigma_{OPLs} = 2\sigma_{zs}$  versus  $\sigma_{OPLi} = 2\sigma_{zi}$  obtained at the single-wavelength  $\lambda_i$ , as written in Eq. 8.

$$\sigma_{OPLs} = \frac{\Lambda}{2\pi} \sigma_{\Phi} = \frac{\sqrt{2}\Lambda}{2\pi} \sigma_{\varphi_i} = \sqrt{2} \frac{\Lambda}{\lambda_i} \sigma_{OPLi} \quad (8)$$

Now inserting for example our experimental values  $\lambda_{average} \sim 670$  nm and  $\Lambda = 16.84$   $\mu\text{m}$  in Eq. 8 directly gives the topographic noise amplification factor  $\sigma_{zs}/\sigma_{zi} = \sigma_{OPLs}/\sigma_{OPLi}$  of about 35, corresponding to the 70 nm beat-wavelength standard deviation versus the single-wavelength 2 nm value. This drawback is therefore very limiting for the raw beat-wavelength measure, because even if the measurement range has been increased in the upper side, the axial resolution does not lie in the nanometer-range anymore. Hopefully, ways to maintain the 2 nm precision for the beat-wavelength imaging, under certain noise conditions, exist and are studied in the next section 3.

### 3. HIGH-RESOLUTION DUAL-WAVELENGTH UNWRAPPING

#### 3.1 Principle of dual-wavelength unwrapping

As seen before, the beat-wavelength phase map obtained by dual-wavelength measurements is able to remove phase ambiguity on an extended range, although it comes at a price of a noise amplification (see Eq. 8). Despite already interesting results that can be obtained with raw beat-wavelength imaging, a lot of applications still request the nanometer-range precision of DHM. In addition to this, the true goal with dual-wavelength approach is to really extend the measurement range of DHM, and not only shift it upwards while losing the interferometric precision advantage.

In summary, the presented method is able to maintain the nanometer-scale resolution when working with the beat-wavelength generated by the two simultaneously-acquired wavefronts of wavelengths  $\lambda_1$  and  $\lambda_2$ . This technique essentially consists in using the beat-wavelength phase map  $\Phi$  only to solve the phase ambiguity for one wavelength, then adding the correct integer multiple of  $2\pi$  to the corresponding single-wavelength phase map  $\varphi_i$ , thus conserving the low-noise characteristics of it. This can be best described as a “dual-wavelength unwrapping” and such algorithms have already been used for sequential two-wavelengths DHM<sup>18,19,28</sup> for a while. Here we propose the implementation of Eq. 9 to retrieve the high-precision unwrapped reflection topographic map  $z_{i,uw} = OPL_i/2$  corresponding to wavelength  $\lambda_i$ .

$$2z_{i,ceil} = \left\lceil \frac{\Phi\Lambda}{2\pi\lambda_i} \right\rceil \lambda_i + \frac{\varphi_i}{2\pi} \lambda_i$$

$$z_i = \begin{cases} z_{i,ceil} & \text{if } |2z_i - \frac{\Phi\Lambda}{2\pi}| < \lambda_i/2 \\ z_{i,ceil} - \lambda/4 & \text{if } |2z_i - \frac{\Phi\Lambda}{2\pi}| > \lambda_i/2 \end{cases}$$

where  $\lceil \cdot \rceil$  the rounder value to the higher integer, and  $z_i = OPL_i/2$  are topographic values.

In Eq. 9, the case serve to have the value of  $z_i$  the closest to the beat-wavelength topography. Consequently, this dual-wavelength algorithm is able to overcome the amplified phase error due to noise on  $\varphi_1$  and  $\varphi_2$ , and theoretically guarantees that the topographic noise remains similar to single-wavelength measurements.

### 3.2 Experimental validation on calibrated step

To validate the technique, the unwrapping method is applied on the high certified step ( $4.463 \pm 0.059 \mu\text{m}$ ) by using the reconstruction phase presented in Fig. 4a-c. The resulting image is presented in Fig. 4d. A comparison of the topographic measurement achieved with the standard phase difference and the unwrapping procedure can be seen on Fig. 5 that presents the profiles obtained along the white line drawn on Fig. 4d. By considering the average value between pixels  $[0,400]$  and  $[550,800]$ , the step height is  $4.4307 \pm 0.1129 \mu\text{m}$  for the phase difference and  $4.4650 \pm 0.0080 \mu\text{m}$  for the unwrapping profile (the incertitude is the sum of the height standard deviation of the value inside the considered intervals). This last value shows that the measured step high with the unwrapping procedure is perfectly in the certified value.

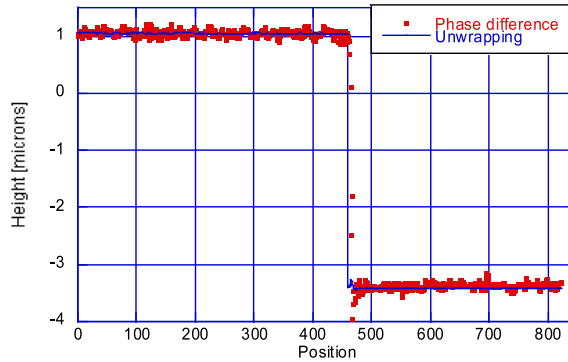


Figure 5. Height measurement obtained from phase difference or after the application of the unwrapping procedure

## 4. UNWRAPPING OF SYNTHETIC PHASE WITH TOPOGRAPHIC MEASUREMENT

### 4.1 Principle and method

The unwrapping method was applied for mapping small wavelength measurement on higher synthetic wavelength. Now we will demonstrate that the  $2\pi$  ambiguity on the synthetic wavelength can also be suppressed by using height measurement achieved with another technique that has a greater measurement range. Obviously, to perform the unwrapping, the precision on the topographic measurement has to be smaller than the synthetic wavelength. Here we will demonstrate the feasibility of the principle by using the vertical scan module implemented on the same DHM R1100<sup>TM</sup> used for the previous results. The basic principle of the vertical scan module is to use short coherence source (suppression of the wavelength filters) and to detect the maximum fringes contrast during the z-scan of the specimen or the OPL scan. A typical vertical scan measurement achieved on the certified step is presented in Fig. 6a.

To unwrap the synthetic phase with the vertical scan measurement, the same method presented in Eq. 9 is applied but the synthetic phase measurement is replaced by the vertical scan measurement and the single wavelength phase by the synthetic phase:

$$\begin{aligned}
 2H_{ceil} &= \left\lceil \frac{2h_{scan}}{\Lambda} \right\rceil \Lambda + \frac{\Phi\Lambda}{2\pi} \\
 H &= \begin{cases} H_{ceil} & \text{if } |2H - 2h_{scan}| < \Lambda/2 \\ H_{ceil} - \Lambda/4 & \text{if } |2H - 2h_{scan}| > \Lambda/2 \end{cases} \quad (9)
 \end{aligned}$$

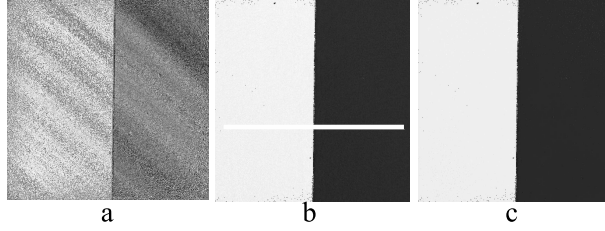


Figure 6. (a) vertical scan measurement; synthetic phase mapped on vertical scan and (c) single phase mapped on (b).

where  $H$  is the unwrapped height and  $h_{scan}$  the height measured by the vertical scan process. Fig. 6b presents the unwrapped synthetic phase. It is evident that the single wavelength measurement can be mapped on the unwrapped synthetic phase to perform a nanometric precision on a higher range than the half of the synthetic wavelength as presented on Fig. 6c and on graph of Fig. 7.

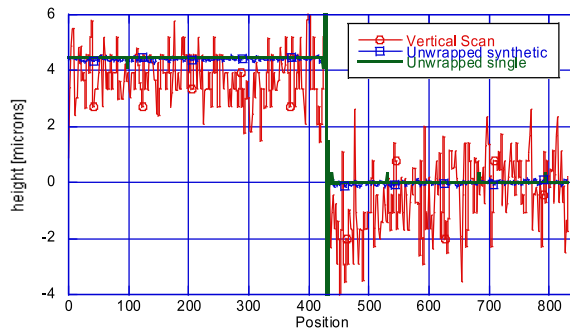


Figure 7. Height measurement obtained from vertical scan and unwrapping of the synthetic phase and single wavelength phase along the white line drawn on Fig. 6b.

## 4.2 Range limitations

Using another measurement, like vertical scan, to unwrap the synthetic wavelength phase, allows to increase significantly the measurement range with nanometric resolution. But the range is not infinite and the first limitation is the coherence of the sources. Indeed, if the specimen is higher than half the coherence length, DHM fails to measure the specimen. Typically, by considering the used wavelength filters ( $\Delta\lambda = 1.3\text{nm}$ ), the coherence lengths are  $L_{c,\lambda_1} = \lambda^2/\Delta\lambda = 360\mu\text{m}$  and  $L_{c,\lambda_2} = 330\mu\text{m}$ . The maximum height that can be measured by dual-wavelength DHM is therefore  $\min(L_{c,\lambda_1}, L_{c,\lambda_2}) = 330\mu\text{m}$ . Of course, this maximum height can be greater by using sources with higher coherence length, But one can note that there is a compromise between the coherence length of the source and the vertical resolution. Indeed, parasitic interferences could occur if the coherence length is too long.

A second important limitation that influences the imaging quality is the depth of field of the MO. Indeed, if the sample is higher than the depth of field, only some parts of the specimen are in focus and the unwrapping procedures (on synthetic or on topographic measure) will not be as effective as usual. Nevertheless, DHM offers the possibility to reconstruct all in focus images. Ferraro *et al.* have already demonstrates that it is possible to reconstruct an extended focused amplitude image from 2D numerical unwrapping phase image.<sup>29</sup> Using the dual-wavelength unwrapping (eventually by using a topographic external measurement as vertical scan), we can reconstruct an all focus complex wavefront; therefore not only an extended focused amplitude but also an extended focused phase image. By using these kind of technique, the depth of field limitation disappears.

## 5. CONCLUSION

In conclusion, the presented approach enables to extend the DHM measurement range to micro-meter range without the inherent limitations of unwrapping algorithms, while keeping the single-wavelength nanometer-range

resolution. The high axial resolution can only be saved if some noise conditions are fulfilled, namely the higher the desired axial range (beat-wavelength) the lower the single-wavelength phase noise should be. Furthermore, we demonstrate that DHM can take advantage to other topographic measurement as vertical scan, to suppress the  $2\pi$  ambiguity on the single wavelength measurement but also on the synthetic wavelength to give theoretically a measurement range about  $300\mu\text{m}$  with a sub-nanometric resolution.

### Acknowledgments

The development of the technology has been supported by Swiss government through CTI grants TopNano 21 #6101.3 and NanoMicro #6606.2 and #7152.1, Swiss National Science Foundation (SNSF) grant #205320-103885/1 and funding from the European Community's Seventh Framework Programme FP7/2007-2013 under grant agreement n° 216105 Real 3D.

### REFERENCES

- [1] Schnars, U. and Jüptner, W., "Direct recording of holograms by a ccd target and numerical reconstruction," *Applied Optics* **33**(2), 179–181 (1994).
- [2] CuChe, E., Bevilacqua, F., and Depeursinge, C., "Digital holography for quantitative phase-contrast imaging," *Optics Letters* **24**(5), 291–293 (1999).
- [3] CuChe, E., Marquet, P., and Depeursinge, C., "Simultaneous amplitude-contrast and quantitative phase-contrast microscopy by numerical reconstruction of fresnel off-axis holograms," *Applied Optics* **38**(34), 6994–7001 (1999).
- [4] Forrester, A. T., Parkins, W. E., and Gerjuoy, E., "On the possibility of observing beat frequencies between lines in the visible spectrum," *Physical Review* **72**(8), 728–728 (1947).
- [5] Hildebrand, B. P. and Haines, K. A., "Multiple-wavelength and multiple-source holography applied to contour generation," *Journal of the Optical Society of America* **57**(2), 155–162 (1967).
- [6] Zelenka, J. S. and Varner, J. R., "A new method for generating depth contours holographically," *Applied Optics* **7**(10), 2107–2110 (1968).
- [7] Wyant, J. C., "Testing aspherics using two-wavelength holography," *Applied Optics* **10**(9), 2113–2118 (1971).
- [8] Polhemus, C., "Two-wavelength interferometry," *Applied Optics* **12**(9), 2071–2074 (1973).
- [9] Bien, F., Camac, M., Caulfield, H. J., and Ezekiel, S., "Absolute distance measurements by variable wavelength interferometry," *Applied Optics* **20**(3), 400–402 (1981).
- [10] Dändliker, R., Thalmann, R., and Prongué, D., "Two-wavelength laser interferometry using superheterodyne detection," *Optics Letters* **13**(5), 339–341 (1988).
- [11] Tiziani, H. J., Rothe, A., and Maier, N., "Dual-wavelength heterodyne differential interferometer for high-precision measurements of reflective aspherical surfaces and step heights," *Applied Optics* **35**(19), 3525–3533 (1996).
- [12] Lu, S.-H. and Lee, C.-C., "Measuring large step heights by variable synthetic wavelength interferometry," *Measurement Science and Technology* **13**(9), 1382–1387 (2002).
- [13] Fercher, A. F., Hu, H. Z., and Vry, U., "Rough surface interferometry with a two-wavelength heterodyne speckle interferometer," *Applied Optics* **24**(14), 2181–2188 (1985).
- [14] Onodera, R. and Ishii, Y., "Two-wavelength interferometry that uses a fourier-transform method," *Applied Optics* **37**(34), 7988–7994 (1998).
- [15] Suzuki, T., Yazawa, T., and Sasaki, O., "Two-wavelength laser diode interferometer with time-sharing sinusoidal phase modulation," *Applied Optics* **41**(10), 1972–1976 (2002).
- [16] Pedrini, G., Froning, P., Tiziani, H. J., and Gusev, M. E., "Pulsed digital holography for high-speed contouring that uses a two-wavelength method," *Applied Optics* **38**(16), 3460–3467 (1999).
- [17] Wagner, C., Osten, W., and Seebacher, S., "Direct shape measurement by digital wavefront reconstruction and multiwavelength contouring," *Optical Engineering* **39**(1), 79–85 (2000).
- [18] Gass, J., Dakoff, A., and Kim, M. K., "Phase imaging without  $2\pi$  ambiguity by multiwavelength digital holography," *Optics Letters* **28**(13), 1141–1143 (2003).

- [19] Parshall, D. and Kim, M., “Digital holographic microscopy with dual wavelength phase unwrapping,” *Applied Optics* **45**(3), 451–459 (2006).
- [20] Colomb, T., Montfort, F., Kühn, J., Aspert, N., Cuche, E., Marian, A., Charrière, F., Bourquin, S., Marquet, P., and Depeursinge, C., “Numerical parametric lens for shifting, magnification and complete aberration compensation in digital holographic microscopy,” *Journal of the Optical Society of America a-Optics Image Science and Vision* **23**(12), 3177–3190 (2006).
- [21] de Nicola, S., Finizio, A., Pierattini, G., Alfieri, D., Grilli, S., Sansone, L., and Ferraro, P., “Recovering correct phase information in multiwavelength digital holographic microscopy by compensation for chromatic aberrations,” *Optics Letters* **30**(20), 2706–2708 (2005).
- [22] Yamaguchi, I., Yamamoto, K., Mills, G. A., and Yokota, M., “Image reconstruction only by phase data in phase-shifting digital holography,” *Applied Optics* **45**(5), 975–983 (2006).
- [23] Mahon, R. J., Murphy, J. A., and Lanigan, W., “Digital holography at millimetre wavelengths,” *Optics Communications* **260**(2), 469–473 (2006).
- [24] Kühn, J., Colomb, T., Montfort, F., Charrière, F., Emery, Y., Cuche, E., Marquet, P., and Depeursinge, C., “Real-time dual-wavelength digital holographic microscopy with a single hologram acquisition,” *Optics Express* **15**(12), 7231–7242 (2007).
- [25] Cuche, E., Marquet, P., and Depeursinge, C., “Spatial filtering for zero-order and twin-image elimination in digital off-axis holography,” *Applied Optics* **39**(23), 4070–4075 (2000).
- [26] Colomb, T., Kühn, J., Charrière, F., Depeursinge, C., Marquet, P., and Aspert, N., “Total aberrations compensation in digital holographic microscopy with a reference conjugated hologram,” *Optics Express* **14**(10), 4300–4306 (2006).
- [27] de Groot, P. and Kishner, S., “Synthetic wavelength stabilization for two-color laser-diode interferometry,” *Applied Optics* **30**(28), 4026–4033 (1991).
- [28] Schnars, U. and Juptner, W. P. O., “Digital recording and numerical reconstruction of holograms,” *Measurement Science and Technology* **13**(9), R85–R101 (2002).
- [29] Ferraro, P., Grilli, S., Alfieri, D., Nicola, S. D., Finizio, A., Pierattini, G., Javidi, B., Coppola, G., and Striano, V., “Extended focused image in microscopy by digital holography,” *Optics Express* **13**(18), 6738–6749 (2005).